Title

Cell type–specific functions of nucleic acid-binding proteins revealed by deep learning on co-expression networks

Naoki Osato [1*] and Kengo Sato [1]

[1] School of Life Science and Technology, Institute of Science Tokyo, Tokyo, Japan.

E-mail: naokiosato11@gmail.com

*Corresponding author.

Abstract

Nucleic acid-binding proteins (NABPs) exhibit cell type–specific regulatory functions, but their target genes and biological roles remain incompletely characterized due to the limitations of current experimental approaches. Here, we present a deep learning framework that integrates gene co-expression correlations to predict NABP regulatory targets and infer their functions across diverse cellular contexts, without requiring binding motif information. By substituting low-informative input features in a transcriptome-based prediction model with co-expression-derived interactions, we achieved improved accuracy in gene expression prediction. Functional enrichment analysis revealed biologically meaningful annotations consistent with known NABP roles. In parallel, we applied a ChatGPT-assisted interpretation framework that provided functional predictions based on semantic patterns among gene sets—an approach that enhances interpretability even for modestly sized sets. Predictions supported by both statistical enrichment and ChatGPT-based inference were less likely to reflect spurious associations, reinforcing their biological relevance. Collectively, this integrative framework—combining deep learning, co-expression networks, and generative AI—enables the systematic discovery of both known and previously uncharacterized NABP functions in a cell type–specific manner.

Keywords

Computational biology, Deep learning, Gene expression, Gene regulation, Protein function prediction

Introduction

Understanding the cell type–specific regulatory functions of nucleic acid-binding proteins (NABPs), including both DNA-binding proteins (DBPs) and RNA-binding proteins (RBPs), remains a fundamental challenge in molecular biology [1-10]. Although experimental assays such as ChIP-seq and ChIA-PET can map DBP binding sites, they require high-quality antibodies and are not easily scalable across large sets of proteins or conditions. The challenge is even greater for RBPs, many of which lack well-defined binding motifs due to their reliance on intrinsically disordered regions (IDRs) for RNA recognition, rather than sequence-specific contacts [11-13]. Interpreting low-affinity DBP binding, which contributes to enhancer activity and paralog-specific regulation, is particularly difficult—especially in the context of phase-separated transcriptional condensates [14]. Conventional methods like eQTL mapping or DNase-seq require prior motif knowledge and struggle to resolve such indirect or context-dependent interactions [15-17]. While massively parallel reporter assays (MPRAs) and large language model–based architectures such as Enformer have advanced our ability to relate sequence to function [18,19], they do not reveal which NABPs mediate the predicted regulatory effects. Thus, novel strategies are required to infer NABP–target relationships and functional roles, particularly when motif information is unavailable or direct binding evidence is missing.

Deep learning has substantially improved the prediction of gene expression by modeling regulatory inputs from NABPs, including transcription factors and microRNAs (miRNAs) [20]. For example, models incorporating ChIP-seq–derived NABP binding sites in promoter regions and predicted miRNA-binding sites in transcripts have achieved a high correlation (r = 0.82) between predicted and observed expression levels. In a previous study, we extended this approach by incorporating binding site data for DNA-

binding proteins within 1 Mb of transcription start sites (TSSs) in open chromatin, while excluding miRNAs and RBPs. To facilitate accurate computation of importance scores (also known as contribution scores) and to improve model interpretability, we unified the input representation by excluding a previous input layer for RNA-binding proteins and miRNAs [21]. While this modification slightly reduced predictive accuracy (r = 0.70), it enabled broader coverage of distal regulatory elements and laid the foundation for downstream functional analysis based on importance scores. These scores are later leveraged to identify regulatory targets and infer NABP functions.

Gene co-expression analysis, a well-established method since the 2000s, offers a complementary perspective by identifying genes with coordinated expression across biological contexts [22-30]. These patterns, derived from transcriptomic datasets across diverse cell types, can capture both direct and indirect regulatory associations—including those involving NABPs with uncertain or difficult-to-characterize binding features. In this study, we integrated gene co-expression data into a deep learning framework to assess its utility for predicting gene expression and identifying context-specific regulatory targets of NABPs. This combination provides a flexible means to infer functional relationships even when direct binding data are lacking.

To test the effectiveness of this approach, we substituted the binding site features of ~300 NABPs that contributed little to previous deep learning predictions with gene co-expression–based interactions. The modified model successfully predicted gene expression levels while assigning DeepLIFT-based importance scores to NABP–gene interactions. Many predicted targets overlapped with ChIP-seq or eCLIP-validated binding partners and showed higher importance scores than background interactions. Functional enrichment analyses of ten representative NABPs revealed consistent

correspondence with known annotations in UniProt [31], and several additional functions were supported by independent publications. To enhance interpretability, we also applied a ChatGPT-based method to infer gene functions and retrieve supporting literature. The results were consistent with enrichment-based findings and highlighted biologically meaningful associations such as circadian rhythm regulation (AKAP8) and glycolysis (PKM).

This study provides a computational strategy to uncover the functional roles and regulatory targets of NABPs without requiring experimentally defined binding sites. By integrating gene co-expression profiles with deep learning, the framework captures both direct and indirect interactions often missed by conventional methods. This approach enables the systematic and scalable identification of NABP functions, providing a new avenue for exploring transcriptional regulation in a cell type–specific manner.

Results

Gene co-expression features enhance expression prediction accuracy

Replacing low-contribution DBP inputs with gene co-expression data led to a substantial increase in model performance (**Fig. 1**). In human foreskin fibroblasts (HFFs), substituting 302 out of 1,310 DBPs with co-expression profiles improved the correlation between predicted and actual gene expression from 0.70 to 0.80 (**Fig. 2a, b**). These co-expression inputs included both NABP-encoding and non-NABP mRNAs, with gene symbols for DNA- and RNA-binding proteins obtained from the ENPD (Eukaryotic Nucleic acid Binding Protein) database[32], and co-expression profiles sourced from COXPRESdb [22]. A subsequent experiment replaced 325 low-contribution DBPs with

108 co-expression interactions involving RBPs, resulting in a further increase in prediction
109 accuracy (r = 0.81; **Fig. 2c**). Collectively, these findings demonstrate that integrating co-
110 expression interactions into the model enhances its ability to capture gene regulatory
111 dynamics beyond direct binding site information.

112 Contribution scores calculated from co-expression–based NABP–gene interactions
113 showed increased variability and notably higher mean and median values than those of
114 the original feature set (**Fig. 2d**, **Supplementary Table S1**). Correlation analysis further
115 revealed consistent relationships between these contribution scores and $\log_2$-transformed
116 transcript expression levels across cell types (**Supplementary Fig. S2**). Example plots
117 demonstrated that the model adjusted its predictions in a cell type–specific manner, with
118 contribution scores reflecting the strength of inferred NABP regulatory influence **(Fig.**
119 **2e**).

120

121 Experimental binding data support model-inferred regulatory targets

122 Experimentally validated binding sites are consistent with deep learning–derived
123 regulatory targets. Genes with ChIP-seq or eCLIP peaks for a given NABP exhibited
124 disproportionately high or low importance ranks, indicating that experimentally
125 confirmed binding sites are associated with stronger regulatory influence in gene
126 expression prediction models. This relationship supports the biological validity of
127 DeepLIFT-based contribution scores, which quantify the importance of specific NABPs
128 in driving gene expression changes.

129 To evaluate this association, we analyzed ChIP-seq data for 32 DBPs in HepG2
130 cells and eCLIP data for 29 RBPs in K562 cells—two cell lines with the most
131 comprehensive publicly available NABP binding site datasets from ENCODE and related

132 studies. A gene was considered associated with an NABP if a ChIP-seq peak was located
133 within ±5 kb of its transcription start site (TSS) or if an eCLIP peak was mapped to its
134 transcribed region. As illustrated in **Fig. 3a** and **Supplementary Fig. S1**, NABPs with
135 experimentally mapped binding sites consistently showed higher absolute values of
136 contribution scores across their predicted target genes, reinforcing their regulatory
137 relevance and aligning with prior interpretations of DeepLIFT scores [20,33].

138 Model-derived importance scores reliably predict DBP binding sites, as evidenced
139 by significant overlap with ChIP-seq peaks. To evaluate this correspondence, we
140 analyzed ChIP-seq data for 32 DNA-binding proteins (DBPs) and quantified how
141 frequently high-scoring gene regions—defined by DeepLIFT contribution scores—
142 coincided with experimental binding evidence. Overlap ratios were calculated as the
143 proportion of high-contribution regions that intersected with ChIP-seq peaks, considering
144 both promoter-proximal (±5 kb) and distal (±100 kb) regions around transcription start
145 sites (TSSs). To account for the functional heterogeneity and abundance of ChIP-seq
146 peaks, we applied a precision-at-K approach, focusing on the top-ranked or top-scoring
147 gene regions most likely to reflect regulatory relevance. Four thresholds were used to
148 define high-contribution regions: two based on contribution score rank (top/bottom 20 or
149 50) and two based on absolute score magnitude (≥ 0.01 or ≤ -0.01; ≥ 0.001 or ≤ -0.001).
150 A control analysis using randomly selected gene regions of matched size was conducted
151 in parallel. In all tested conditions, the overlap between ChIP-seq peaks and high-
152 contribution regions exceeded that of the random control, supporting the model's ability
153 to prioritize functionally relevant regulatory sites (**Fig. 3b**).
154

Deep learning uncovers functionally enriched NABP target genes beyond co-expression networks

Model-predicted regulatory targets of nucleic acid-binding proteins (NABPs) display consistent functional enrichment patterns, highlighting the biological specificity of the deep learning approach (**Table 1, 2** and **Supplementary Note**). To evaluate the functional consistency of these predicted targets, we conducted Gene Ontology (GO) enrichment analysis on ten representative NABPs [34,35]. The selected gene sets demonstrated statistically significant enrichment for functionally related GO terms, in contrast to randomly sampled gene sets of equivalent size, which did not exhibit such enrichment (**Fig. 4**). Importantly, comparison with all co-expressed genes (Pearson's *z*-score > 2) revealed that the model-selected subsets contained enriched annotations not statistically detectable in the broader co-expression profiles. This suggests that the deep learning model filters co-expression signals to identify a biologically focused set of target genes. Functional enrichment was confirmed using the PANTHER Overrepresentation Test across multiple annotation resources, including GO Slim, Reactome, and PANTHER Pathways (**Table 1**) [36]. To complement these results, we applied a ChatGPT-based gene set interpretation method (**Table 2** and **Supplementary Note**) [37], which inferred functions and retrieved literature consistent with the GO-based findings and UniProt annotations [31]. Notably, AKAP8 was linked not only to its known role in the mitotic cell cycle (UniProt) but also to circadian clock regulation, supported by literature associating AKAP8 with molecular clock genes and melatonin biosynthesis (**Fig. 5** and **6**; **Supplementary Table S4** and **Supplementary Note**) [38]. For this analysis, AKAP8's top 50 predicted targets were defined by ranking all genes according to their model-derived NABP contribution scores, and selecting those for which AKAP8 received the highest

179 score in K562 cells. These results demonstrate that integrating co-expression–guided
180 deep learning with large language model–based interpretation yields robust insights into
181 both canonical and previously unrecognized biological functions of NABPs.

182 Deep learning–based refinement of NABP–target predictions enhances the
183 detection of biologically specific functional annotations. To evaluate how training
184 influences functional specificity, we compared GO term enrichment between co-
185 expressed gene sets and predicted regulatory targets for ten NABPs. Although the co-
186 expressed gene sets were larger and exhibited broader enrichment, several functionally
187 informative annotations were uniquely or more significantly enriched among the deep
188 learning–derived target genes **(Table 3**, **Supplementary Table S4** and **S5**). For instance,
189 circadian rhythm–related functions linked to AKAP8 and kinase- or glycolysis-related
190 annotations associated with PKM were observed only following model training (**Table 3**
191 and **Supplementary Table S4**) [39-42]. For PKM, we defined 332 predicted targets by
192 ranking all genes according to NABP contribution scores and selecting those for which
193 PKM ranked within the top two contributors. These results suggest that the model
194 captures biologically meaningful signals beyond simple expression correlations.
195 Importantly, both PKM and AKAP8 are RNA-binding proteins whose functional
196 predictions were derived from a deep learning model trained on gene expression data
197 from K562 cells—a human erythroleukemia cell line widely used in leukemia research.
198 This contextual consistency provides biological credibility to the inferred functions.
199 ALDOA, a glycolysis-associated partner of PKM, and AKAP8, linked to circadian gene
200 networks, have both been implicated in leukemia metabolism and clock regulation,
201 underscoring the relevance of these functions to K562 biology [38,43-46]. Furthermore, the
202 ChatGPT-based functional inference retrieved consistent biological themes—"circadian

203 clock" for AKAP8 and "glycolysis" for PKM—reinforcing the deep learning–based
204 predictions through independent, literature-derived validation (**Fig. 5** and **6**) [37].
205 In neuronal cells, however, AKAP8 exhibited minimal predicted regulatory activity,
206 in contrast to its circadian-linked role in cancer. The model identified very few AKAP8
207 targets in the neuronal context, which limited downstream functional annotation by both
208 PANTHER and ChatGPT-based interpretation. This was based on a contribution score–
209 based ranking across all genes, where only four genes had AKAP8 ranked as the top
210 contributor, and two genes had AKAP8 ranked among the six lowest-scoring NABPs.
211 These findings suggest that AKAP8 may have limited transcriptional influence in neurons,
212 reinforcing its potential role as a context-dependent regulator.
213 PKM exhibits distinct regulatory profiles in cancer and neuronal cells, reflecting
214 divergent metabolic adaptations. In K562 cancer cells, PKM is associated with a
215 Warburg-like metabolic reprogramming, as indicated by the significant enrichment of
216 aldolase activity among its predicted targets, notably including ALDOC and TALDO1
217 (**Supplementary Table S4**) [47,48]. TALDO1, a key enzyme in the non-oxidative branch of
218 the pentose phosphate pathway, contributes to nucleotide biosynthesis and redox balance,
219 supporting the proliferative and survival needs of cancer cells. This metabolic shift is
220 correlates with the activation of the hypoxia-inducible factor (HIF) pathway, involving
221 HIF1A, VEGFA, BNIP3, and DDIT4, which collectively enhance glycolysis,
222 angiogenesis, and adaptation to hypoxic conditions (**Supplementary Note**) [49,50]. In
223 contrast, in neuronal cells, ALDOC—but not TALDO1 or ALDOA—was among the
224 predicted PKM-regulated genes, and aldolase activity was not significantly enriched
225 (**Supplementary Table S4**) [51]. For this analysis, 326 predicted targets were selected
226 based on NABP contribution scores, where PKM ranked among the top two contributors

227 per gene. This suggests that neuronal PKM (predominantly PKM1) maintains a stable
228 glycolytic flux to support basal ATP production, rather than engaging in metabolic
229 reprogramming [52,53]. Furthermore, although several HIF-responsive genes (e.g., EGLN1,
230 BNIP3, MIR210HG) were among the predicted targets, HIF1A itself was not, indicating
231 a context-dependent modulation of the HIF axis in neurons. Collectively, these findings
232 suggest that PKM is repurposed across cell types, integrating core metabolic programs
233 with distinct transcriptional partners tailored to tissue-specific functional demands.

234 Finally, the integration of deep learning-based co-expression modeling with AI-
235 assisted literature mining enabled functional predictions even for less thoroughly
236 characterized regulators such as AKAP8. This framework supports both hypothesis
237 generation and validation across cell types, and highlights the utility of scalable,
238 interpretable tools for deciphering context-specific gene regulatory logic.

239

240

241 **Discussion**

242 These findings address a long-standing challenge in molecular biology: the
243 systematic functional characterization of nucleic acid-binding proteins (NABPs) across
244 diverse cellular contexts. While traditional methods rely heavily on experimental binding
245 data and known motifs, our approach utilizes gene co-expression and machine learning
246 to circumvent these limitations. By capturing both direct and indirect regulatory signals,
247 it broadens the scope of functional prediction for NABPs that lack conventional binding
248 site information.

249 Gene expression correlations alone can serve as a powerful basis for uncovering
250 the regulatory roles of nucleic acid-binding proteins (NABPs), even in the absence of

251 experimental binding data. Leveraging transcriptomic profiles from diverse public RNA-
252 seq datasets, our deep learning framework inferred regulatory targets of NABPs based
253 solely on co-expression patterns. Unlike binding site assays such as ChIP-seq or eCLIP—
254 which are technically demanding and limited by the availability of high-quality
255 antibodies—this computational approach is scalable and applicable across NABPs with
256 poorly characterized binding motifs. Functional enrichment analysis of the predicted
257 target genes revealed biologically meaningful roles, many of which were in agreement
258 with existing annotations in public databases. Additionally, several novel functional
259 associations—not found in UniProt or GO but supported by published literature—were
260 uncovered. These findings were further corroborated using a ChatGPT-assisted literature
261 mining method, which retrieved consistent biological themes and references. Together,
262 these results underscore the biological relevance of NABP–target predictions based on
263 gene expression correlations and demonstrate the value of integrating deep learning with
264 AI-assisted interpretation. This strategy offers a scalable path toward elucidating NABP
265 functions and discovering new regulatory mechanisms across diverse cellular contexts.

266 In cancer cells, AKAP8 appears to serve as a molecular integrator of transcriptional
267 regulation under environmental stress. Our analyses, combined with recent reports,
268 suggest that AKAP8 may support hypoxic adaptation through its interaction with DDX5,
269 a multifunctional RNA helicase known to promote HIF-1 transcriptional activity (**Fig. 6**)
270 [54]. DDX5 enhances the recruitment of HIF-1α/β heterodimers to hypoxia-responsive
271 elements (HREs), thus facilitating the expression of genes involved in glycolysis,
272 angiogenesis, and cell survival under low oxygen conditions [55]. Notably, AKAP8 has
273 been shown to physically interact with DDX5 in lung carcinoma cells, forming a
274 chromatin-associated complex that modulates R-loop stability and transcriptional

275 dynamics [56]. Given that DDX5 levels decrease under hypoxia, yet their re-expression
276 restores aberrant R-loop accumulation, AKAP8 may function as a stabilizing co-factor
277 that compensates for transcriptional stress in hypoxic tumor microenvironments. In
278 addition to hypoxia-associated functions, AKAP8 is also implicated in circadian rhythm
279 regulation. In our study, AKAP8 was identified as a potential regulator of circadian genes
280 in K562 cancer cells, and ChatGPT-based inference retrieved functional annotations such
281 as "circadian clock" and "rhythm." Prior studies have linked the disruption of circadian
282 timing systems to tumor progression [57], suggesting that AKAP8 may contribute to
283 temporal dysregulation in cancer. Thus, AKAP8 may play dual roles by coupling
284 chromatin-associated RNA processing to both metabolic and temporal regulatory circuits
285 in malignancies. Taken together, these findings position AKAP8 as a context-dependent
286 regulatory hub that coordinates hypoxia response and circadian control through
287 interaction with DDX5 and possibly other nuclear partners. Targeting such
288 multifunctional scaffolds may offer new strategies for modulating tumor cell plasticity
289 and transcriptional resilience in the face of environmental stress.

290 A key feature distinguishing cancer cells from non-proliferative cells such as
291 neurons is their ability to reprogram core metabolic pathways to support growth under
292 hypoxic and nutrient-limited conditions. Our analysis supports the presence of a PKM2–
293 HIF-1−ALDOC/TALDO1 regulatory axis in cancer cells (**Fig. 6**) [58-61], which coordinates
294 glycolytic and pentose phosphate pathway gene expression to enable metabolic flexibility.
295 Notably, although ALDOA is a well-established glycolytic enzyme and a known PKM
296 interactor in human and mouse (STRING database), it was not among the PKM co-
297 expressed genes in our K562 transcriptomic data (Pearson's z-score < 2), whereas
298 ALDOC—typically regarded as a brain-specific isoform—emerged as a strongly co-

299 expressed and PKM-regulated gene. This suggests that ALDOC may functionally
300 substitute for or complement ALDOA in hematopoietic contexts. In agreement with this,
301 transcriptomic profiles from the Human Protein Atlas indicate that both ALDOA and
302 ALDOC are expressed in K562 cells, raising the possibility that PKM2 may preferentially
303 regulate ALDOC under hypoxia, while ALDOA may operate independently or through
304 non-PKM-mediated control. Functionally, ALDOC contributes to anaerobic glycolysis
305 and has been implicated in chemoresistance and tumor cell survival, while TALDO1, a
306 key enzyme in the non-oxidative branch of the pentose phosphate pathway, facilitates
307 carbon flux recycling and supports NADPH and nucleotide biosynthesis—functions
308 essential for redox balance and proliferation under stress. These roles are consistent with
309 their upregulation in various cancer models under hypoxic conditions. In contrast,
310 neuronal cells predominantly express the PKM1 isoform, which sustains a high-
311 efficiency glycolytic flux coupled to mitochondrial oxidative phosphorylation. In our
312 neuronal cell model, ALDOC—but not ALDOA or TALDO1—was predicted as a PKM-
313 regulated gene, and no significant enrichment for aldolase activity was detected. This
314 underscores the metabolic priorities of neurons, which emphasize consistent ATP supply
315 over biosynthetic plasticity, and exhibit minimal reliance on the HIF-1 pathway. The
316 absence of HIF1A among PKM targets in neurons further supports the notion of a
317 transcriptionally uncoupled hypoxic response in these cells. Together, these findings
318 reveal how PKM isoform usage and gene network context shape distinct metabolic wiring
319 across cell types. In cancer, PKM2 engages in metabolic reprogramming through the
320 selective regulation of genes like ALDOC and TALDO1 to support hypoxia-adaptive and
321 proliferative states. In neurons, PKM1 maintains homeostatic energy production under
322 physiological conditions. The selective engagement of ALDOC in both contexts—but

323 through divergent regulatory logic—highlights a potential metabolic node of interest,
324 while the lack of ALDOA co-expression with PKM suggests a context-dependent
325 separation of biochemical and transcriptional control. These insights may inform future
326 strategies to exploit tumor-selective metabolic dependencies.

327 Contribution scores derived from gene expression correlations capture both direct
328 and indirect regulatory interactions, offering insights beyond what ChIP-seq alone can
329 provide. While ChIP-seq detects thousands of DNA-binding events per protein, many of
330 these sites do not contribute directly to gene expression regulation and may reflect the
331 multifunctionality of transcription factors [62,63]. Consequently, ChIP-seq–derived binding
332 maps and DeepLIFT-based predictions show only partial overlap, underscoring both
333 methodological differences and the inherent complexity of regulatory networks. In this
334 study, gene co-expression analysis revealed fewer target genes than ChIP-seq but
335 identified subsets that are likely to be more functionally relevant. Our previous work on
336 insulator-associated factors linked such proteins to enhancer–promoter insulation and
337 chromatin organization, including phase separation and loop formation [21]. That study
338 incorporated eQTL data to anchor binding sites to expression outcomes. Here, by contrast,
339 we focused on NABPs with unknown motifs and excluded motif-based or chromatin
340 accessibility data such as DNase-seq or ATAC-seq, to assess the capacity of gene
341 expression correlations to reveal regulatory roles. Notably, the distribution of
342 contribution scores for co-expression–based inputs included both high and low values,
343 implying that gene expression patterns reflect not only direct binding but also indirect
344 regulation mediated through broader network effects. This highlights the value of
345 contribution scores as indicators of both proximal and distal regulatory influences, even
346 when binding motifs are unknown or experimental binding data are unavailable.

Functional roles of NABPs can be inferred even from small gene sets, provided that the target genes exhibit shared or functionally related patterns. In this study, ten NABPs showed functional enrichments consistent with known annotations, supporting the validity of the deep learning–based predictions. These enrichments were identified using Fisher's exact test with false discovery rate (FDR) correction via the PANTHER database, which typically requires at least 50 genes for robust statistical significance. For proteins with fewer than 50 predicted targets, enrichment may be harder to detect depending on the functional composition of the gene set. Relaxing the ranking thresholds increased the number of target genes and enhanced statistical power. Alternatively, more stringent thresholds could be retained if the contribution scores were sufficiently strong, offering flexibility depending on analysis goals. Additional features—such as gene expression levels or co-expression correlations—could further refine enrichment analyses, particularly for borderline cases. Notably, enrichment analysis of both high- and low-ranking targets revealed candidate novel functions for specific NABPs, suggesting that genes with large-magnitude contribution scores are biologically informative. Moreover, a complementary ChatGPT-based approach demonstrated utility in interpreting small gene sets. Unlike standard enrichment tools, this method can infer biological roles even when gene counts fall below conventional significance thresholds, provided that genes with related functions are present. This capacity helps overcome statistical limitations and broadens the interpretability of regulatory predictions in a cell type–specific context.

Strategic use of co-expression data enhances functional inference, while indiscriminate replacement can diminish biological relevance. The selective integration of gene co-expression data improved target prediction and the functional interpretability of the model. In contrast, replacing all input features with co-expression-derived

371 interactions led to a decrease in enriched annotations, and known functional roles were
372 no longer recovered. Excessive replacement of input features with gene co-expression
373 data further diminished the biological relevance of model predictions. When all NABP–
374 target inputs were substituted with co-expression-based interactions, the number of
375 enriched functional annotations declined, and previously identified functions from the
376 UniProt database were no longer recovered. This suggests that indiscriminate
377 replacement may cause the model to capture non-informative or biologically spurious
378 associations. A similar trend was observed in a prior control analysis, where substituting
379 true regulatory targets with randomly selected genes led to a gradual loss of enrichment
380 as randomness increased. Based on these observations, the normalized count of enriched
381 functional terms—adjusted by the number of predicted targets—may serve as a useful
382 proxy for evaluating the accuracy and biological validity of NABP–target predictions [64].
383 These findings also raise intriguing questions about how the deep learning model
384 prioritizes informative input features during training. Future work exploring the model's
385 internal representation dynamics—such as how it distinguishes signal from noise when
386 presented with diverse regulatory interactions—may provide valuable insights into the
387 mechanisms of transcriptional regulation and model interpretability. Investigating how
388 the model converges on biologically meaningful NABP–target relationships during
389 training—possibly through attention mechanisms or layer-wise relevance propagation—
390 could deepen our understanding of both gene regulation and model interpretability.

391 Cell type specificity and cooperative binding dynamics may underlie the absence
392 of detectable regulatory signals for certain NABPs. While some NABPs showed no
393 high- or low-ranking target genes in HepG2 or K562 cells, such absence does not rule out
394 regulatory relevance. These proteins may exhibit cell type–specific regulatory activity

395 detectable only in other cellular contexts, where functional enrichment analysis could
396 reveal distinct biological roles. Moreover, many transcription factors and DNA-binding
397 proteins act in concert, forming multi-protein complexes that bind cooperatively to shared
398 promoters [65-67]. In such cases, individual components may not always yield strong
399 contribution scores due to their distributed regulatory influence across the complex. This
400 highlights the potential of co-binding site analysis as a complementary strategy to uncover
401 cooperative regulatory mechanisms and to disentangle the functional interplay of NABPs
402 within transcriptional networks.

403 This study establishes a scalable computational framework for uncovering the
404 functional roles of nucleic acid-binding proteins (NABPs) using gene expression
405 correlations and deep learning. By leveraging co-expression–based interactions and
406 contribution scoring, the model successfully identified both canonical and novel
407 regulatory associations across cell types—even in the absence of experimentally defined
408 binding motifs. The results highlight how expression-driven inference, complemented by
409 AI-assisted functional interpretation, can advance our understanding of NABP biology
410 beyond conventional binding site–centered approaches. Although the present analysis
411 focused on a representative subset of proteins and cell types, the framework is readily
412 adaptable to broader transcriptomic datasets and larger NABP cohorts. As such, it offers
413 a path forward for systematic annotation of NABPs, particularly those with poorly
414 characterized regulatory roles. Together, these findings provide a foundation for future
415 studies to decode complex gene regulatory architectures and integrate transcriptomic and
416 AI-driven predictions into functional genomics research at scale.
417
418

419 # Methods

420 ## Predictive modeling of gene expression across diverse cell types using
421 deep learning and NABP binding information

422 To predict gene expression across multiple human cell types, we adapted a
423 previously established deep learning framework that integrates DNA-binding site data for
424 transcription factors and other regulatory proteins. In this implementation, regulatory
425 elements located both proximally and distally (up to ±1 Mb) from transcription start sites
426 (TSSs) were included as input features (**Fig. 1**) [20,21]. To minimize the effects of cellular
427 heterogeneity in bulk tissue, RNA-seq datasets were selected at the individual cell-type
428 level. Publicly available RNA-seq data were retrieved for four functionally distinct cell
429 types: human foreskin fibroblasts (HFFs), mammary epithelial cells (HMECs), neural
430 progenitor cells (NPCs), and either HepG2 hepatoma cells or K562 leukemia cells,
431 depending on the class of regulatory protein analyzed [68,69]. Gene expression values
432 (FPKM) were computed using the RSeQC toolkit based on GENCODE v19 annotations,
433 and subsequently $\log_2$-transformed after adding a small offset to avoid undefined values.
434 Following the approach described by Tasaki et al. [20,21], expression fold changes were
435 calculated relative to the median expression level across the four cell types. For each
436 model iteration, three common cell types (HFFs, HMECs, and NPCs) were used, and
437 either HepG2 (for DNA-binding protein analysis) or K562 (for RNA-binding protein
438 analysis) was included to match the availability of ChIP-seq and eCLIP validation
439 datasets. These cell types were chosen to represent diverse biological lineages and
440 regulatory contexts.

441

442

Extended regulatory features and DeepLIFT-compatible model design

To capture distal regulatory signals beyond promoter regions, we integrated DNA-binding site data from putative enhancers into a deep learning framework for gene expression prediction. Building upon our earlier work [20,21], this model extends the architecture originally proposed by Tasaki et al. (2020) [20,21], which focused on promoter-proximal regions and included RNA-binding protein and miRNA inputs. In our previous study, aimed at identifying insulator-associated DNA-binding proteins, we deliberately excluded RNA-binding proteins and miRNAs to focus on DNA-centered regulatory elements. Instead, we combined DNA-binding sites from both promoter (-2 kb to +1 kb) and enhancer-like regions (±1 Mb from the transcription start site [TSS]) into a unified input matrix, enabling DeepLIFT analysis under the high-accuracy "genomics-default" mode.

Binding site coordinates were obtained from the GTRD database (v20.06) [70], and regulatory associations were inferred using cis-eQTLs from GTEx v8. A ChIP-seq peak that overlapped a 100-bp window centered on an expression-associated SNP was considered linked to the corresponding transcript. Trans-eQTLs were excluded, and coordinates were converted to the hg19 assembly using UCSC LiftOver [71]. To limit feature dimensionality while maximizing genomic coverage, we computed peak lengths for each DNA-binding protein (DBP) in 100-bp bins across ±1 Mb around the TSS, then retained the maximum peak value within each 10-kb window, yielding up to 200 enhancer bins. These were concatenated with 30 promoter-region bins to form a 230-bin unified input layer. This single-input-layer structure was necessary because DeepLIFT's genomics-default configuration ("RevealCancel rule on dense layers and Rescale rule on conv layers") does not support models with multiple input layers. Concatenating all DBP-

467 related features into one matrix thus maintained compatibility while enhancing
468 interpretability.

469 Model training followed the protocol described by Tasaki et al. and applied in our
470 prior work [20,21]. Specifically, 2,705 genes from chromosome 1 were used for testing,
471 while 22,251 genes from other chromosomes were randomly assigned to the training set
472 and 2,472 to the validation set. Models were implemented in TensorFlow 2.6.0 and
473 trained on an NVIDIA RTX 3080 GPU, typically completing in 2 to 4 hours. Feature
474 importance was assessed using DeepLIFT, which assigned contribution scores to input
475 features indicating their relative influence on gene expression prediction.

476

477 Predicting NABP regulatory targets using gene co-expression–informed 478 substitutions

479 To uncover regulatory targets of NABPs without relying on direct binding site
480 assays, we implemented a co-expression–driven modification of the deep learning input.
481 Specifically, DNA-binding proteins with low contribution scores in the original model
482 were replaced with NABPs whose regulatory interactions were inferred from gene co-
483 expression data. Of the 1,310 DBPs initially included, 302 were substituted with other
484 DBPs, and in a separate RNA-binding protein analysis, 325 were replaced with RNA-
485 binding proteins (RBPs) identified from the ENPD database [32]. Putative NABP–target
486 relationships were established using co-expression profiles provided by COXPRESdb [22],
487 where a Pearson's *z*-score > 2 between a NABP-encoding gene and a non-NABP gene
488 indicated a strong co-expression link. These co-expression pairs served as proxies for
489 regulatory interactions and were used to generate new input features for the model. To
490 integrate these proxies into the deep learning framework, hypothetical NABP binding

491 sites were assigned at the transcription start site (TSS) and 2 kb upstream of each co-
492 expressed gene. The model was then retrained using this modified input, and DeepLIFT
493 was applied to calculate importance scores, evaluating the influence of each NABP–gene
494 interaction on predicted expression levels. This approach enables the functional
495 characterization of NABPs with unknown or uncharacterized binding motifs by
496 leveraging gene co-expression as a proxy for regulatory targeting.
497

498 Prioritization of NABP regulatory targets based on importance score 499 rankings

500 To identify the primary regulatory targets of each NABP, genes were ranked
501 based on the importance scores assigned to NABP binding sites by the deep learning
502 model. Genes with binding sites consistently ranked in the top five or bottom five across
503 all NABPs were selected as putative targets, reflecting high positive or negative
504 regulatory influence. These targets represent genes most strongly associated with a given
505 NABP's regulatory activity. To ensure sufficient statistical power for downstream
506 enrichment analysis, rank thresholds were adjusted for each NABP based on the number
507 of high-confidence predictions. While a contribution score rank cutoff of five was
508 sufficient in most cases, the threshold was relaxed in specific cases—for example, up to
509 rank eight for proteins such as RPLP0, which initially yielded a smaller number of
510 predicted targets.

511 Functional enrichment and AI-based interpretation confirm the biological
512 relevance of NABP regulatory targets. To evaluate the biological coherence of predicted
513 NABP regulatory targets, we performed functional enrichment analysis using the
514 Statistical Overrepresentation Test from the PANTHER database alongside custom in-

515 house scripts [36]. Gene Ontology (GO) terms from biological process, molecular function,
516 and cellular component categories were analyzed for enrichment across three gene sets:
517 (1) primary regulatory target genes identified by the model, (2) all co-expressed genes
518 (Pearson's *z*-score > 2), and (3) randomly selected genes of matched size. Enrichment
519 was assessed using Fisher's exact test with Benjamini–Hochberg false discovery rate
520 (FDR) correction, and FDR < 0.05 was considered statistically significant. For this
521 analysis, human gene symbols were mapped to Ensembl Gene IDs using the HGNC
522 database (https://www.genenames.org/), and GO annotations were obtained from the
523 Gene Ontology resource [34,35]. Target gene IDs served as the test set, while the full
524 expression dataset used in the deep learning model formed the reference background. To
525 complement the statistical analysis, we applied a ChatGPT-based functional inference
526 method [37]. This approach used curated prompts—detailed in *Extended Data Tables 1 and*
527 *5*—to predict functional roles based on gene sets, and retrieved relevant literature using
528 a modified version of the "4.Reference search and validation.ipynb" script [37]. This script
529 is publicly available on Code Ocean and GitHub
530 (https://doi.org/10.24433/CO.7045777.v1 ;
531 https://github.com/idekerlab/llm_evaluation_for_gene_set_interpretation). The
532 ChatGPT-based results provided consistent and interpretable biological themes aligned
533 with the enrichment findings.
534

535 Validation of predicted NABP targets using experimentally determined 536 binding

537 To assess the biological relevance of the predicted regulatory targets, we
538 compared deep learning–inferred NABP–gene associations with experimentally

539 validated binding data. Specifically, we evaluated the spatial overlap between predicted
540 target genes and ChIP-seq peaks for 32 DNA-binding proteins (within ±5 kb of
541 transcription start sites [TSSs]) as well as eCLIP peaks for 29 RNA-binding proteins
542 (within the transcribed region from TSS to transcription end site [TES]). Gene structure
543 annotations were derived from the GENCODE v19 release [72], and binding site data were
544 obtained from the ENCODE portal and prior publications (**Supplementary Table S6**) [73].
545 This overlap analysis provides orthogonal validation for the predicted targets and
546 supports the utility of gene co-expression–based modeling for inferring NABP–target
547 relationships.
548

549 ## Statistical analysis

550 Functional enrichment was assessed using Fisher's exact test, with multiple testing
551 correction applied via the Benjamini–Hochberg false discovery rate (FDR) procedure.
552 Statistical significance was defined as FDR < 0.05. Distributions of DeepLIFT
553 contribution scores for nucleic acid-binding sites derived from gene co-expression data
554 and ChIP-seq data were compared using the Mann–Whitney U test (also known as the
555 Wilcoxon rank-sum test). A p-value < 0.05 was considered statistically significant.
556

557 ## Data availability

558 RNA-seq data for human foreskin fibroblast (HFF) cells were obtained from the Gene
559 Expression Omnibus (GEO) under accession number GSM941744. RNA-seq data for
560 human mammary epithelial cells (HMEC) were retrieved from ENCODE via the UCSC
561 Genome Browser (http://genome.ucsc.edu/encode/) under the file name
562 *wgEncodeCshlLongRnaSeqHmecCellPapAlnRep1.bam*. RNA-seq data for human neural

progenitor cells (NPC) were obtained from GEO under accession number GSM915326. RNA-seq data for HepG2 and K562 cells were obtained from the ENCODE portal under accession numbers ENCFF670LIE and ENCFF584WML, respectively. mRNA co-expression data were downloaded from COXPRESdb v7 (https://zenodo.org/record/6861444). The list of nucleic acid-binding proteins was obtained from the Eukaryotic Nucleic acid Binding Protein (ENPD) database (http://qinlab.sls.cuhk.edu.hk/ENPD/). ChIP-seq data for transcription factors were downloaded from the GTRD database (v20.06 release; https://gtrd.biouml.org). eQTL data (GTEx_Analysis_v8_eQTL.tar) were obtained from the GTEx portal (v8 release; https://gtexportal.org). eCLIP data for RNA-binding proteins were retrieved from the ENCODE portal (accession ENCSR456FVU) and from Supplementary Data 2 of Van Nostrand et al., *Nature* (2020), https://doi.org/10.1038/s41586-020-2077-3.

Code availability

The deep learning model implemented in this study is available at https://github.com/reposit2/coexgene.

Figures

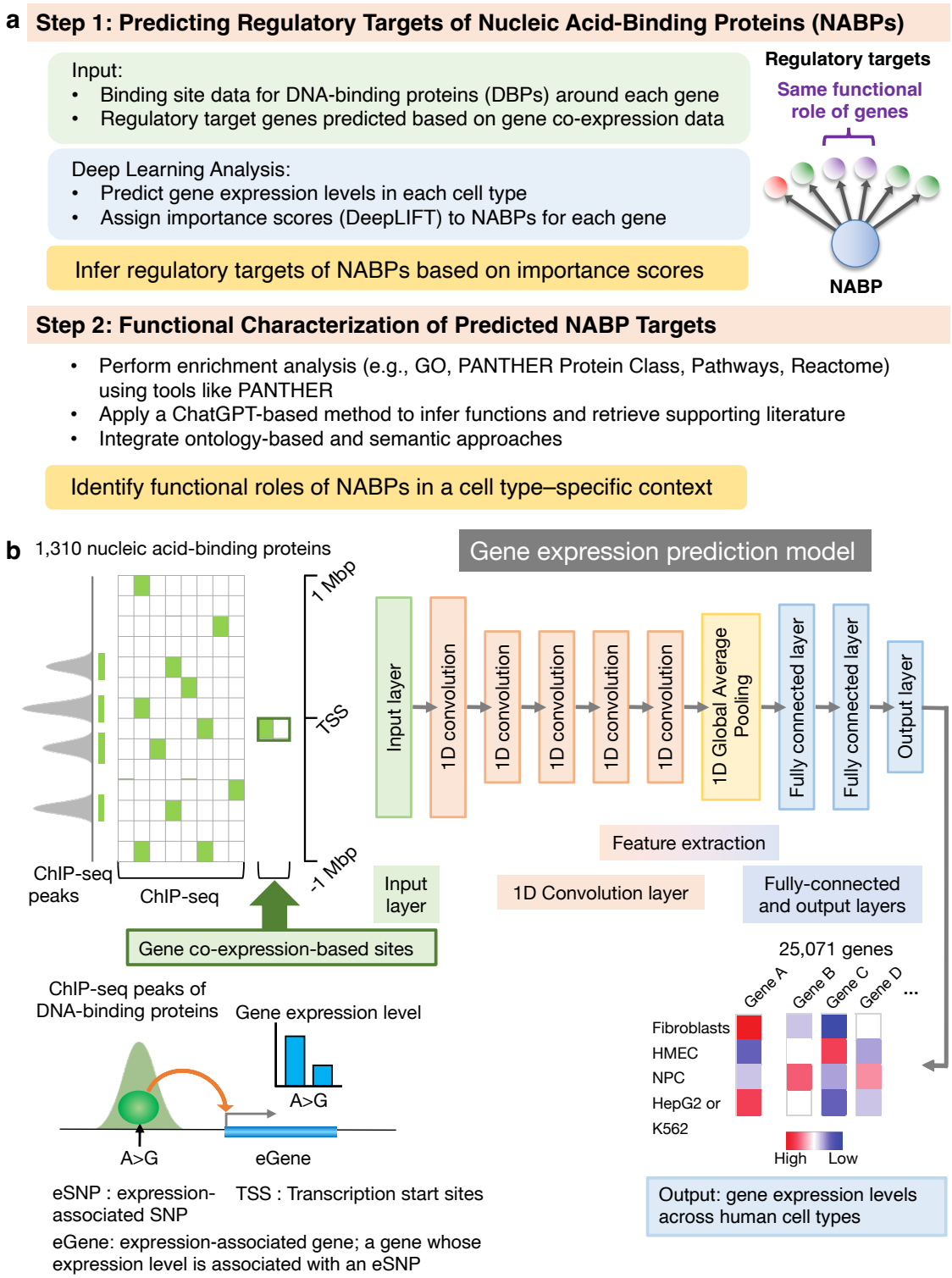

Figure 1. Overview of the deep learning framework for predicting and functionally characterizing NABP regulatory targets.

a. This diagram outlines the overall strategy used to infer the functional roles of nucleic acid-binding proteins (NABPs) from gene expression data. Gene expression profiles from various human cell types were integrated with NABP–gene co-expression relationships derived from COXPRESdb. These inferred interactions were used to replace low-contribution DNA-binding proteins in a deep learning model originally trained on ChIP-seq–based binding site data. The modified model was trained to predict gene expression levels and identify regulatory target genes using DeepLIFT-derived importance scores. Functional annotations of the predicted target genes were assessed using both conventional enrichment analysis and a ChatGPT-based method for literature-guided interpretation.

b. Gene expression levels in human cells were predicted using the genomic locations of DNA-binding sites at promoters and distal elements.

During model training, a DNA-binding protein bound to a distal region overlapping an expression-associated SNP (eSNP) was linked to a potentially regulated gene (eGene) based on eQTL data. For each gene–protein pair, ChIP-seq peak locations were binned (indicated by green boxes) and formatted into a matrix as input for deep learning.

In co-expression–based models, binding sites were artificially assigned near transcription start sites (TSSs). The deep learning model consisted of 1D convolutional layers, global average pooling, and fully connected layers. It predicted gene expression levels across 25,071 genes and multiple human cell types.

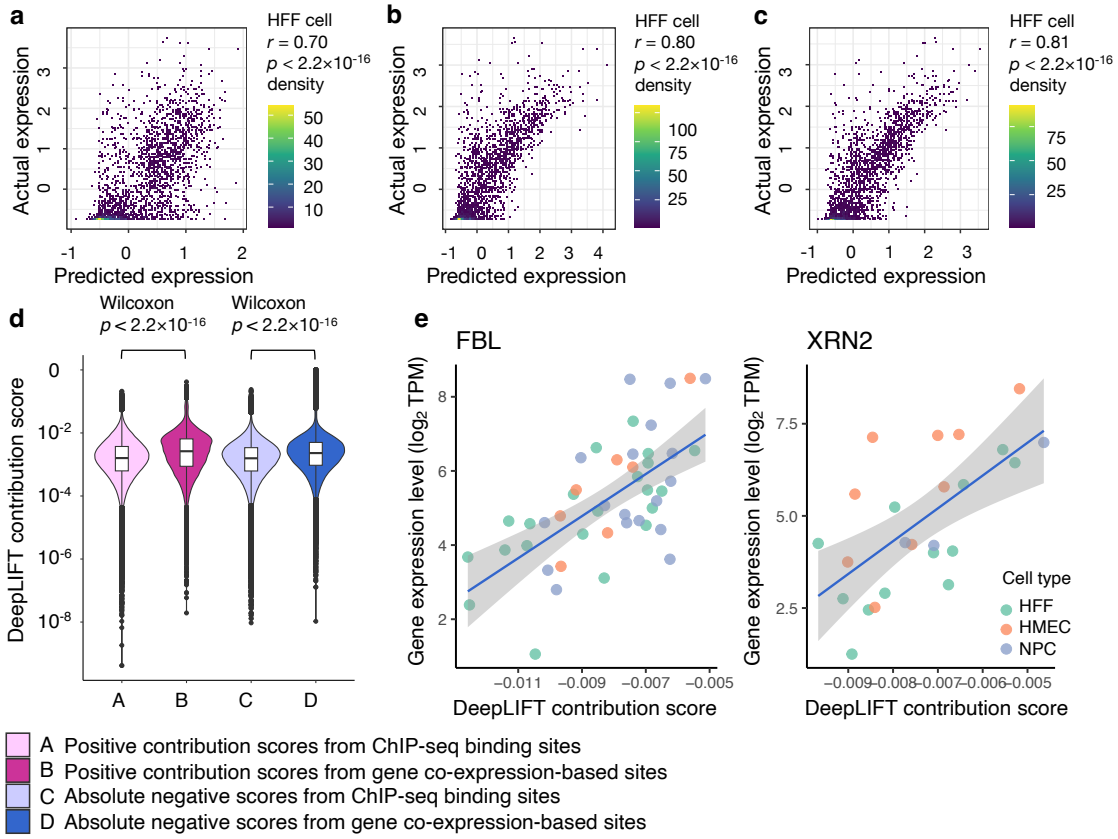

Figure 2. Relationship between gene expression levels and contribution scores. Gene expression levels ($\log_2$ TPM) predicted by a deep learning model were compared with actual expression levels in HFF cells using Spearman's rank correlation.

a. Input features included DNA-binding sites of 1,310 proteins obtained from ChIP-seq data.

b. Among these, 302 proteins with low contribution scores were replaced by an equal number of DNA-binding proteins identified based on gene co-expression.

c. Similarly, 325 DNA-binding proteins were replaced with RNA-binding proteins identified from co-expression relationships.

d. DeepLIFT contribution scores were significantly higher for binding sites derived from gene co-expression data compared to those from ChIP-seq data (Wilcoxon signed-rank

test, $p < 2.2 \times 10^{-16}$). Panels a and b show distributions of positive contribution scores, while C and D show absolute values of negative contribution scores.

e. Representative examples illustrating the correlation between a regulator's DeepLIFT contribution score and the expression levels of its predicted target genes. Linear regression lines with 95% confidence intervals are shown.

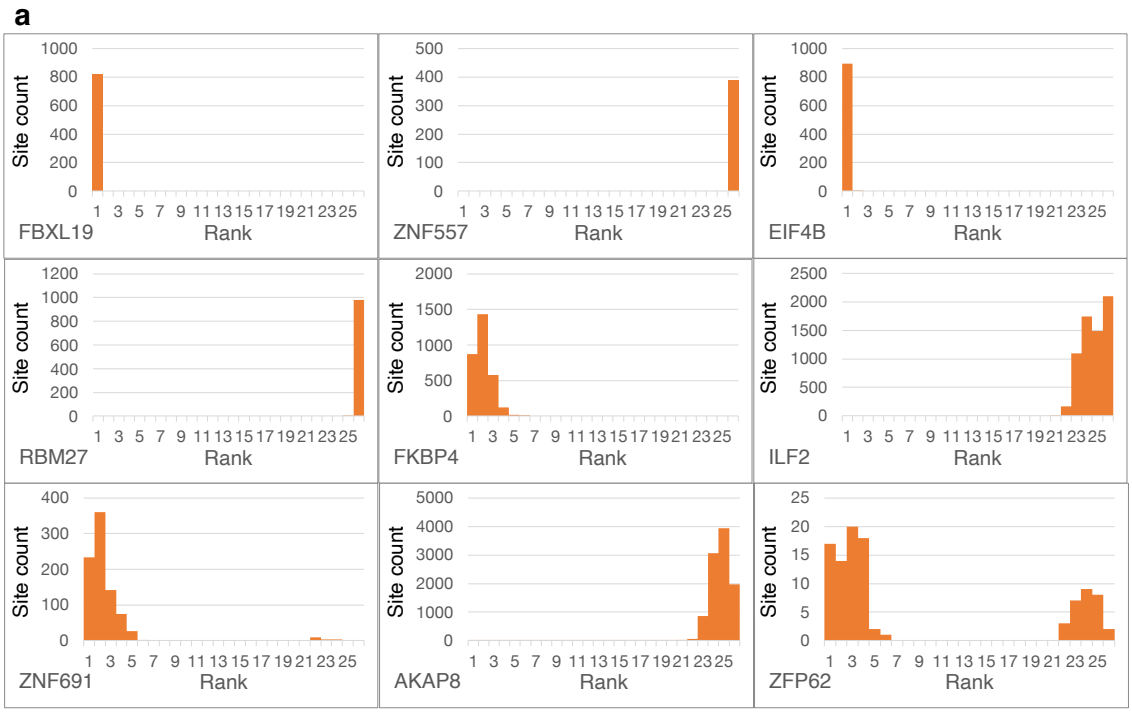

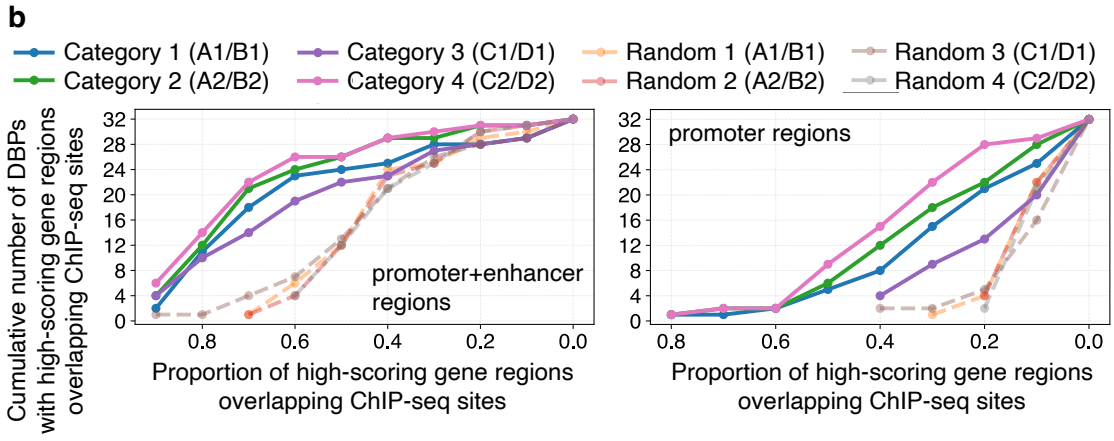

Figure 3. Comparison of predicted regulatory target genes with experimental ChIP-seq and eCLIP binding data. This figure illustrates how predicted gene-level regulatory contributions derived from deep learning correspond to experimentally identified nucleic acid-binding protein targets across genomic regions.

a. Distribution of contribution scores across ChIP-seq–identified binding sites. The x-axis indicates the rank of contribution scores assigned to nucleic acid-binding sites used to predict gene expression levels. Scores were ranked from 1 (highest positive contribution, left) to 1,310 (lowest negative contribution, right) and binned into 50-rank intervals. Rank 1 corresponds to ranks 1–50, rank 2 to ranks 51–100, and rank 26 to ranks 1,251–1,310. Nucleic acid-binding sites were classified as being located within promoters or transcribed regions of genes experimentally bound by the nucleic acid-binding protein depicted in each panel. These sites showed higher or lower contribution scores than those across all ChIP-seq binding sites. The y-axis indicates the number of sites within each 50-rank bin. Positive contribution scores are indicative of gene activation, whereas negative scores reflect gene repression.

b. Proportion of high-contribution gene regions overlapping ChIP-seq binding sites in promoter + enhancer and promoter-only regions, relative to all high-contribution regions. Labels indicating "promoter + enhancer regions" and "promoter-only regions" are shown above the corresponding panels. The proportion represents the number of high-contribution regions within promoter + enhancer intervals (±100 kb of the transcription start site [TSS]; left panel) and promoter-only intervals (±5 kb of the TSS; right panel) that overlap with ChIP-seq binding sites, divided by the total number of high-contribution regions in each category. To define high- and low-contribution regions, multiple thresholds were applied to the 1,310 DNA-binding proteins analyzed: **Rank-based**

654 **thresholds** — (A1 and B1): rank ≥ 20 or ≤ 1,290; (A2 and B2): rank ≥ 50 or ≤ 1,260.
655 **Score-based thresholds** — (C1 and D1): contribution score ≥ 0.01 or ≤ -0.01; (C2 and
656 D2): contribution score ≥ 0.001 or ≤ -0.001 (see **Supplementary Note and Tables S2**
657 **and S3**).
658
659

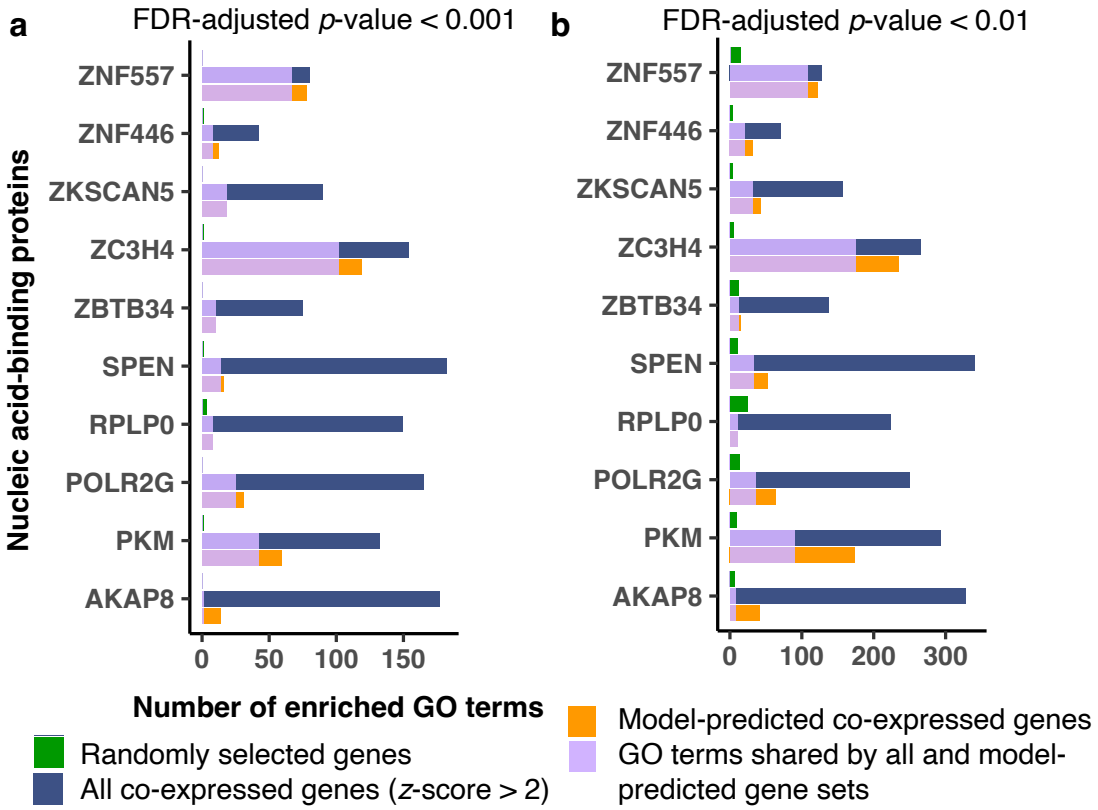

660
661 **Figure 4. Overrepresented functional annotation terms among target genes of**
662 **nucleic acid-binding proteins.**
663 Panels **a** and **b** show results filtered at false discovery rate (FDR)–adjusted *p*-values of
664 < 0.001 and < 0.01, respectively. Functional enrichment analysis was conducted for three
665 gene sets: (1) model-predicted co-expressed genes, (2) all co-expressed genes with a
666 Pearson correlation *z*-score > 2, and (3) randomly selected genes of equal size. Gene

667 Ontology (GO) terms from the categories of biological process, molecular function, and
668 cellular component were combined. Fisher's exact test *p*-values were adjusted using the
669 Benjamini–Hochberg method to control the false discovery rate (FDR).
670
671

AKAP8 (K562 cells)
1. Circadian Control of Metabolic Regulation
This system includes multiple components of the circadian clock (*PER2, PER3, CRY2, NR1D1*), which regulate daily oscillations of gene expression in metabolic tissues. These transcriptional regulators control the rhythmic expression of key metabolic enzymes and transporters, thereby orchestrating the timing of energy storage, mobilization, and hormonal signaling across the light-dark cycle. Their co-presence with nutrient transporters and signaling proteins suggests functional integration in time-dependent metabolic homeostasis.

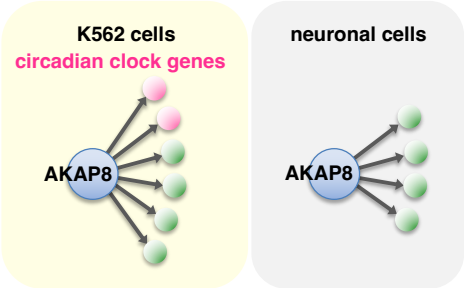

PKM (K562 cells)
1. Hypoxia Sensing and Adaptive Response
This system prominently features components regulated by or regulating **hypoxia-inducible factors (HIFs).** *HIF1A*, *EGLN1*, *EGLN3*, *MIR210HG*, *VEGFA*, *BNIP3*, and *DDIT4* are core mediators of the transcriptional and metabolic response to low oxygen conditions. *EGLNs* hydroxylate HIF1A under normoxia, while *HIF1A* activates genes that enhance glycolytic flux, angiogenesis (*VEGFA*), and survival during hypoxic stress (*BNIP3*, *MIR210HG*). *DDIT4* connects hypoxia to mTOR inhibition, reducing energy expenditure. These factors establish a functional axis adapting metabolism and signaling to oxygen availability.
2. Metabolic Reprogramming Toward Glycolysis
Glycolytic genes including *PFKP*, *PFKL*, *ENO1*, *ENO2*, *ENO3*, *ALDOC*, *LDHA*, and *HK2* are key effectors of the hypoxia-induced metabolic shift. HIF1A upregulates these enzymes, favoring glycolysis and lactate production over mitochondrial respiration. This shift is supported by regulatory components like *PDK1*, *PDK3*, and *SLC16A3* (lactate transporter), which further suppress pyruvate entry into mitochondria and facilitate acid-base balance under anaerobic metabolism.

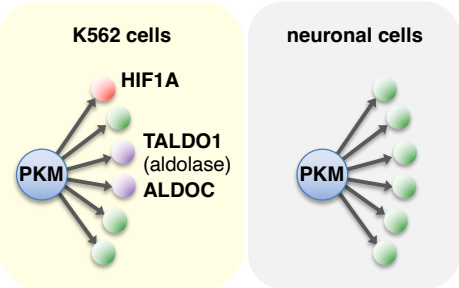

672
673 **Figure 5. Functional mapping of nucleic acid-binding proteins reveals context-**
674 **dependent regulatory roles in cancer and neuronal cells.**
675 A deep learning model trained on transcriptomic co-expression data was used to predict
676 the regulatory influence of nucleic acid-binding proteins (NABPs) on gene expression.
677 Contribution scores were computed to quantify the impact of each NABP across target
678 genes, and the highest-ranking genes were designated as predicted regulatory targets.
679 Functional interpretation was performed using a large language model–based inference
680 method, which identified key biological pathways associated with each NABP. The

resulting schematic highlights the distinct functional roles of AKAP8 and PKM in K562 leukemia cells—circadian regulation and metabolic reprogramming under hypoxia, respectively—in contrast to their more limited or divergent activities in neuronal cells.

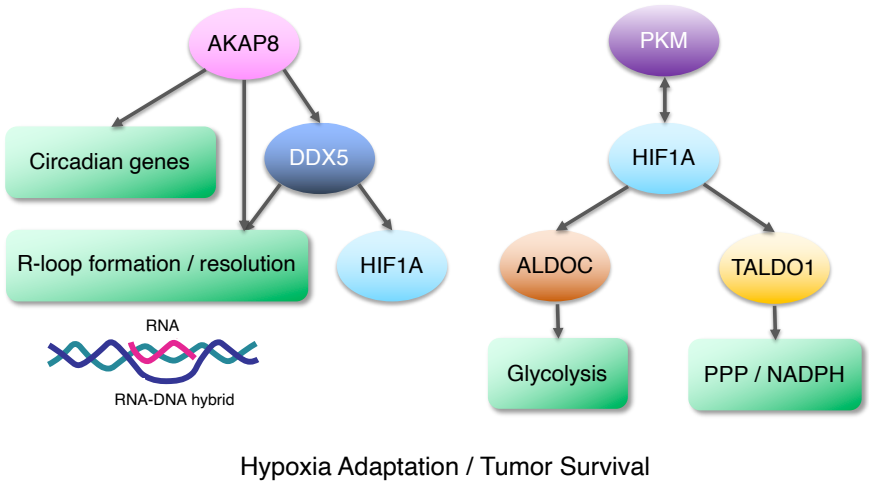

Figure 6. Integrated hypoxia-responsive regulatory network orchestrated by AKAP8 and PKM in cancer cells. This model illustrates how two nucleic acid-binding proteins (NABPs)—AKAP8 and PKM—regulate distinct yet interconnected transcriptional programs to support tumor adaptation under hypoxic stress. AKAP8 acts through DDX5 to influence R-loop resolution [74], circadian gene expression, and the stabilization of HIF1A transcriptional activity. In parallel, PKM modulates HIF1A-driven metabolic reprogramming, promoting glycolysis via ALDOC and redox homeostasis via TALDO1. The predicted regulatory links were inferred from contribution scores calculated by a deep learning framework and are supported by published functional studies in cancer models. PPP: Pentose Phosphate Pathway; NADPH: Nicotinamide Adenine Dinucleotide Phosphate (reduced form).

Tables

Table 1. Functional roles inferred for nucleic acid-binding proteins: integration of UniProt annotations, ChatGPT-based predictions, and confidence scores.

Functional annotations obtained from UniProt entries were systematically compared with significantly enriched biological processes among the model-predicted regulatory targets, as identified by the PANTHER Overrepresentation Test (see **Supplementary Table S4**). Shared or overlapping functions between each nucleic acid-binding protein (NABP) and its predicted targets are indicated. Functional roles inferred using a ChatGPT-based interpretation method are highlighted in yellow, with confidence scores—defined as the proportion of annotated genes within the gene set—provided in parentheses. Confidence levels are categorized as high (0.87–1.00), medium (0.82–0.86), low (0.01–0.81), or none (0). For methodological reference, see Hu M. et al., *Nat. Methods*, 2025 (https://doi.org/10.1038/s41592-024-02525-x) [37].

AKAP8
negative regulation of RNA biosynthetic process
Circadian clock system
Cry-Per complex
Circadian-regulated energy metabolism and insulin signaling (0.74)

PKM
kinase
glycolytic process
ATP metabolic process
Hypoxia-adaptive metabolic remodeling and cell migration (0.79)

POLR2G
RNA polymerase II transcription regulatory region sequence-specific DNA binding
general transcription factor
translational protein
Ribosome biogenesis and RNA maturation at the interface of translation and nuclear export (0.91)

RPLP0
large ribosomal subunit
ribonucleoprotein complex
cytosolic large ribosomal subunit
Mitochondrial-linked ribosome function and RNA-guided surveillance in translational homeostasis (0.84)

SPEN
mRNA binding
chromatin binding
transcription coregulator activity
Chromatin-associated transcriptional regulation and nuclear RNA export integration (0.83)

ZBTB34
C2H2 zinc finger transcription factor
DNA-binding transcription activator activity, RNA polymerase II-specific
RNA polymerase II transcription regulatory region sequence-specific DNA binding
Transcriptional regulation by C2H2 zinc finger proteins and signaling modulation (0.72)

ZC3H4
chromatin/chromatin-binding, or -regulatory protein
transcription regulator activity
metal ion binding
RNA-binding protein–mediated transcriptional integration and pre-mRNA processing (0.89)

ZKSCAN5
DNA-binding transcription factor activity
C2H2 zinc finger transcription factor
RNA polymerase II cis-regulatory region sequence-specific DNA binding
metal ion binding
RNA processing, ribonucleoprotein assembly, and transcription-coupled quality control (0.83)

ZNF446
C2H2 zinc finger transcription factor
extracellular space
Transcription-coupled RNA processing and mitochondrial RNA metabolism (0.81)

ZNF557
DNA-binding transcription activator activity, RNA polymerase II-specific
RNA polymerase II transcription regulatory region sequence-specific DNA binding
ion binding, metal ion binding
Transcriptional regulation and RNA metabolic coordination via zinc finger proteins and RNA-associated complexes (0.88)

Table 2. Functional characterization of predicted regulatory targets of nucleic acid-binding proteins using a ChatGPT-based inference framework.

717 Representative biological functions were inferred for each NABP by applying a large
718 language model–based gene set interpretation method. Functional themes are
719 summarized in bold for each NABP, while numbered subcategories denote distinct
720 functional roles associated with individual gene subsets.
721

AKAP8 (K562 cells)
Circadian-regulated energy metabolism and insulin signaling (0.74)
1. Circadian Control of Metabolic Regulation
2. Insulin Signaling and Glucose Transport
3. Fatty Acid and Lipid Homeostasis
4. Metabolite Transport and Mitochondrial Function
5. Signal Integration and Vesicle Trafficking
6. Developmental and Structural Modulators

PKM (K562 cells)
Hypoxia-adaptive metabolic remodeling and cell migration (0.79)
1. Hypoxia Sensing and Adaptive Response
2. Metabolic Reprogramming Toward Glycolysis
3. Extracellular Matrix Remodeling and Migration
4. Vesicular and Membrane Trafficking
5. Mitochondrial Function and ROS Homeostasis
6. Transcriptional and Epigenetic Regulation

PKM (neuronal cells)
Hypoxia-driven metabolic and structural reprogramming (0.87)
1.Hypoxia Sensing and Transcriptional Response
2.Glycolytic Shift and Mitochondrial Modulation
3.Cytoskeletal Remodeling and Motility Enhancement
4.Endocytosis, Vesicle Transport, and Membrane Dynamics
5.RNA Processing and Translation Control
6.Ubiquitination and Proteostasis
7.Stress Signaling and Nuclear Regulation

POLR2G (K562 cells)
Ribosome biogenesis and RNA maturation at the interface of translation and nuclear export (0.91)
1. Cytoplasmic and Nuclear Ribosomal Component Assembly
2. Ribosomal RNA Processing and Modification
3. Translational Initiation and Ribosome Recycling
4. Proteasome-Linked Ribosome Quality Control
5. Nuclear Export, mRNP Surveillance, and RNA Chaperoning

RPLP0 (K562 cells)
Mitochondrial-linked ribosome function and RNA-guided surveillance in translational homeostasis (0.84)
1. Ribosomal Structural Components and Translational Core
2. RNA Modification and Surveillance by Small Non-Coding RNAs
3. RNA Surveillance and Nuclear Export Quality Control
4. Mitochondrial and Redox-Linked Translational Interface
5. Membrane Trafficking and Endoplasmic Reticulum Integration
6. Zinc Finger Regulators and DNA Repair Coupling

SPEN (K562 cells)
Chromatin-associated transcriptional regulation and nuclear RNA export integration (0.83)
1. Transcriptional Regulation and Chromatin Remodeling
2. RNA Binding, Processing, and Export
3. Protein Quality Control and Ubiquitin-Mediated Regulation
4. Signal-Responsive Transcription Integration
5. RNA Surveillance and Stability
722 6. Nuclear Structural and Trafficking Components

ZBTB34 (HepG2 cells)
Transcriptional regulation by C2H2 zinc finger proteins and signaling modulation (0.72)
1. Transcriptional Regulation by Zinc Finger Proteins
2. Signaling and Transcriptional Crosstalk
3. Modulators of Chromatin and RNA Stability
4. Functional Integration and Cell Fate Control

ZC3H4 (HepG2 cells)
RNA-binding protein–mediated transcriptional integration and pre-mRNA processing (0.89)
1. RNA-Binding Protein Network and Pre-mRNA Processing
2. Transcription-Coupled Regulatory Scaffold
3. Spliceosome Assembly and Dynamic Coordination
4. mRNA Export and Quality Control
5. Epigenetic and Histone Regulatory Interface
6. RNA Modification and Stability Regulation
7. Nucleolar and Ribosome Biogenesis Linkage

ZKSCAN5 (HepG2 cells)
RNA processing, ribonucleoprotein assembly, and transcription-coupled quality control (0.83)
1. RNA Processing and mRNA Surveillance
2. Transcriptional Regulation and Chromatin Remodeling
3. Ribosome Biogenesis and Mitochondrial Translation
4. Protein Quality Control and Ubiquitin-Dependent Regulation
5. Nucleocytoplasmic Transport and Organelle Coordination
6. ZNF and ZBTB Family-Mediated Regulatory Modules

ZNF446 (HepG2 cells)
Transcription-coupled RNA processing and mitochondrial RNA metabolism (0.81)
1. Transcriptional Regulation and Initiation
2. Splicing and RNA Processing
3. Mitochondrial RNA Metabolism and Translation
4. RNA Transport and Nuclear Export
5. Ubiquitin-Proteasome and RNA-Protein Complex Quality Control
6. Chromatin-Linked Transcription Modulators

ZNF557 (HepG2 cells)
Transcriptional regulation and RNA metabolic coordination via zinc finger proteins and RNA-associated complexes (0.88)
1. Transcriptional Regulation by Zinc Finger Proteins
2. General Transcription Machinery and RNA Polymerase Assembly
3. RNA Splicing, Processing, and Surveillance
4. rRNA Processing and Ribosome Biogenesis
5. Epigenetic and Chromatin-Level Regulation
6. Coupling with RNA Modification and Translation Control

723

724

725 **Table 3. Functional enrichments among predicted regulatory target genes of nucleic**

726 **acid-binding proteins.**

727 Functional enrichment analysis was conducted using the PANTHER database. This table

728 lists annotations that were statistically enriched in regulatory target genes predicted by a

729 deep learning model trained on gene co-expression data. These annotations were not

730 significantly overrepresented in the full set of co-expressed genes (Pearson's *z*-score > 2)

731 that included the nucleic acid-binding protein itself. '**Reference**' indicates the total

732 number of human genes; '**Analyzed**' denotes the number of regulatory target genes

733 examined; '**Expected**' represents the number of genes expected to have the annotation by

734 chance; '**Over/Under**' specifies whether the annotation is overrepresented or

735 underrepresented; '**Fold Enrichment**' reflects the observed-to-expected ratio; '**Raw P-**

736 **value**' reports the result of Fisher's exact test; and '**FDR**' refers to the Benjamini–

737 Hochberg false discovery rate.

AKAP8							
PANTHER Pathways							
PANTHER Pathways	Reference (17130)	Analyzed (49)	Expected	Over/ Under	**Fold Enrichment**	raw P-value	FDR
Circadian clock system (P00015)	10	3	0.03	+	> 100	2.60E-06	4.16E-04
PANTHER GO-Slim Biological Process							
PANTHER GO-Slim Biological Process	Reference (17130)	Analyzed (49)	Expected	Over/ Under	**Fold Enrichment**	raw P-value	FDR
circadian regulation of gene expression (GO:0032922)	16	3	0.05	+	65.55	1.20E-05	1.27E-02
response to light stimulus (GO:0009416)	21	3	0.06	+	49.94	2.82E-05	1.99E-02
circadian rhythm (GO:0007623)	21	3	0.06	+	49.94	2.82E-05	1.49E-02
rhythmic process (GO:0048511)	24	3	0.07	+	43.7	4.27E-05	1.81E-02
GO cellular component complete							
GO cellular component complete	Reference (17130)	Analyzed (49)	Expected	Over/ Under	**Fold Enrichment**	raw P-value	FDR
Cry-Per complex (GO:1990512)	3	2	0.01	+	> 100	2.40E-05	4.77E-02
PKM							
PANTHER Protein Class							
PANTHER Protein Class	Reference (17130)	Analyzed (326)	Expected	Over/ Under	**Fold Enrichment**	raw P-value	FDR
aldolase (PC00044)	5	2	0.1	+	21.02	3.48E-03	5.68E-02
kinase (PC00137)	134	9	2.55	+	3.53	1.07E-03	2.62E-02
PANTHER GO-Slim Molecular Function							
PANTHER GO-Slim Molecular Function	Reference (17130)	Analyzed (326)	Expected	Over/ Under	**Fold Enrichment**	raw P-value	FDR
enzyme inhibitor activity (GO:0004857)	107	8	2.04	+	3.93	1.01E-03	4.68E-02
kinase activity (GO:0016301)	562	23	10.7	+	2.15	7.08E-04	3.57E-02
PANTHER GO-Slim Biological Process							
PANTHER GO-Slim Biological Process	Reference (17130)	Analyzed (326)	Expected	Over/ Under	**Fold Enrichment**	raw P-value	FDR
endoplasmic reticulum tubular network organization (GO:0071786)	12	3	0.23	+	13.14	1.32E-03	3.68E-02
regulation of cellular component biogenesis (GO:0044087)	139	10	2.65	+	3.78	3.31E-04	1.05E-02

Acknowledgements

Supercomputing resources were provided by the Human Genome Center, the Institute of Medical Science, the University of Tokyo, and the ROIS National Institute of Genetics.

Author contributions

N.O. designed and conducted the research, and wrote and revised the manuscript. K.S. revised the manuscript.

Supplementary data

Supplementary data are available at

Conflict of interests

None declared.

Funding

This work was supported by the Japan Society for the Promotion of Science (JSPS) KAKENHI [Grant Number 16K00387], a start-up research grant from Osaka University, the KIOXIA Young Scientist Research Grant at Waseda University, the Grant for Basic Science Research Projects from the Sumitomo Foundation, the Research Grant from the CASIO Science Promotion Foundation, and the Research Grant from the Okawa Foundation for Information and Telecommunications awarded to N.O., JST CREST [Grant Number JPMJCR23N1], and the GteX Program Japan [Grant Number JPMJGX23B4] awarded to K.S.

768 **Supplementary Note and Tables**

769

770 **Gene co-expression–based predictions align with ChIP-seq–defined**
771 **DNA-binding targets**

772 High-ranking predicted binding regions frequently coincide with ChIP-seq peaks,
773 particularly in promoter–enhancer intervals. Deep learning–derived DNA-binding site
774 predictions based on gene co-expression data show substantial concordance with ChIP-
775 seq results, particularly when broader genomic regions encompassing promoters and
776 putative enhancers are considered. When overlap was assessed within ±100 kb of
777 transcription start sites (TSSs)—a window supported by prior enhancer–gene mapping
778 studies [19,75]—the mean and median overlap ratios reached 0.69 and 0.76, respectively
779 (Ratio A2 / B2; **Supplementary Tables S2 and S3**). In contrast, overlap was lower for
780 promoter regions alone (±5 kb), with corresponding mean and median values of 0.33 and
781 0.34. Some DNA-binding proteins, including FBXL19, POGK, SPEN, THAP7, ZNF142,
782 and ZNF800, showed notably high promoter-region overlap ratios (>0.5), indicating
783 potential direct regulatory activity. Nevertheless, not all ChIP-seq peaks necessarily
784 reflect functionally relevant transcriptional binding events. Consequently, model-inferred
785 high-scoring sites do not universally coincide with experimentally determined binding
786 regions, underscoring the complexity and context dependence of regulatory interactions.

787

788

789

790

Context-specific predictions reveal known and emerging functional roles of NABPs

The deep learning–based predictions successfully recapitulate both established and potentially novel biological functions of NABPs. For example, AKAP8—previously annotated in UniProt with canonical cell cycle functions (e.g., "GO:0000278 mitotic cell cycle" and "GO:0044839 cell cycle G2/M phase transition")—was also predicted to be associated with circadian rhythm regulation in this study. Supporting literature retrieved from PubMed indicates a potential role for AKAP8 in circadian rhythm control: one study identified AKAP8 as strongly co-expressed with core clock genes such as *CRY1*, while another reported its involvement in melatonin biosynthesis, a pathway that is often disrupted in individuals with autism spectrum disorders [76,77].

PKM (pyruvate kinase M) was functionally linked to glycolytic regulation, consistent with literature-based protein–protein interaction data, including its experimentally validated interaction with ALDOA in both human and mouse systems [39,40]. However, co-expression analysis in our dataset revealed a notable context-specific pattern: ALDOA and ALDOB were not significantly co-expressed with PKM (Pearson's z-score < 2), whereas ALDOC was identified as a prominently co-expressed gene prior to deep learning model training. This result suggests that ALDOC may serve as a context-dependent effector of PKM-regulated glycolysis, particularly in hematopoietic settings such as K562 cells. Indeed, ALDOC was not only among the predicted regulatory targets of PKM, but also appeared in gene sets annotated with hypoxia-responsive functions involving HIF1A. Moreover, transcriptomic data from the Human Protein Atlas confirmed that both ALDOA and ALDOC are expressed in K562 cells, further supporting the possibility that PKM may selectively regulate ALDOC in specific cellular contexts,

815 despite the known biochemical role of ALDOA in glycolysis. These findings exemplify
816 how deep learning–guided predictions can refine our understanding of tissue-specific
817 metabolic wiring and highlight functional divergence within enzyme families.
818
819
820 **Supplementary Table S1. Co-expression–based selection enhances the**
821 **contribution scores of NABP binding sites.**
822 Binding sites identified through gene co-expression exhibited higher absolute
823 DeepLIFT contribution scores compared to those selected solely from ChIP-seq data
824 without co-expression information. This trend was observed for both DNA-binding
825 proteins in HepG2 cells and RNA-binding proteins in K562 cells. For each group, the
826 table reports the mean and median values of positive and negative contribution scores.
827 These findings suggest that gene co-expression–based selection preferentially identifies
828 functionally impactful regulatory interactions.

DNA-binding proteins (HepG2 cell)			
Co-expression–based		**Non-co-expression–based**	
	Plus score		Plus score
Mean	0.005673	Mean	0.003391
Median	0.003829	Median	0.001893
	Minus score		Minus score
Mean	-0.017000	Mean	-0.002502
Median	-0.002286	Median	-0.001583

RNA-binding proteins (K562 cell)			
Co-expression–based		**Non-co-expression–based**	
	Plus score		Plus score
Mean	0.004916	Mean	0.002962
Median	0.002422	Median	0.001689
	Minus score		Minus score
Mean	-0.011987	Mean	-0.002485
Median	-0.001521	Median	-0.001414

829
830
831
832
833

Supplementary Table S2. Enrichment of high-contribution promoter regions with experimentally validated DBP binding sites. (See Supplementary Excel file)

This table summarizes the proportion of promoter regions (±5 kb from transcription start sites) that were both predicted to be functionally important by DeepLIFT contribution scores and validated by ChIP-seq data for the corresponding DNA-binding proteins (DBPs). Overlap ratios were calculated across four thresholds—two based on rank and two on absolute score—to assess the robustness of the predictions.

To classify high and low contributions, multiple thresholds were applied to the 1,310 DNA-binding proteins analyzed:

Rank-based thresholds:

(A1 and B1) proteins ranked in the top or bottom 20 (i.e., rank ≤ 20 or ≥ 1,290)

(A2 and B2) proteins ranked in the top or bottom 50 (i.e., rank ≤ 50 or ≥ 1,260)

Score-based thresholds:

(C1 and D1) contribution score ≥ 0.01 or ≤ –0.01

(C2 and D2) contribution score ≥ 0.001 or ≤ –0.001

Supplementary Table S3. Enrichment of high-contribution promoter and enhancer regions with ChIP-seq–validated DBP binding sites.

This table presents the proportion of overlap between predicted high-contribution regions (defined within ±100 kb of transcription start sites, covering both promoters and distal enhancers) and ChIP-seq binding sites for the corresponding DNA-binding proteins (DBPs). Strong concordance between model-based predictions and ChIP-seq peaks

858 across multiple thresholds underscores the reliability of the contribution scoring method
859 in identifying functionally relevant regulatory sites.
860 To classify high and low contributions, the following thresholds were applied to
861 the 1,310 DNA-binding proteins analyzed:
862 **Rank-based thresholds**:
863 (A1 and B1) proteins ranked in the top or bottom 20 (i.e., rank ≤ 20 or ≥ 1,290)
864 (A2 and B2) proteins ranked in the top or bottom 50 (i.e., rank ≤ 50 or ≥ 1,260)
865 **Score-based thresholds**:
866 (C1 and D1) contribution score ≥ 0.01 or ≤ –0.01
867 (C2 and D2) contribution score ≥ 0.001 or ≤ –0.001
868
869
870 **References**
871

872 1 Belz, G. T. & Nutt, S. L. Transcriptional programming of the dendritic cell network.
873 *Nature reviews. Immunology* **12**, 101-113, doi:10.1038/nri3149 (2012).
874 2 Miller, J. C. *et al.* Deciphering the transcriptional network of the dendritic cell lineage.
875 *Nature immunology* **13**, 888-899, doi:10.1038/ni.2370 (2012).
876 3 Ravasi, T. *et al.* An atlas of combinatorial transcriptional regulation in mouse and man.
877 *Cell* **140**, 744-752, doi:10.1016/j.cell.2010.01.044 (2010).
878 4 Gertz, J. *et al.* Distinct properties of cell-type-specific and shared transcription factor
879 binding sites. *Molecular cell* **52**, 25-36, doi:10.1016/j.molcel.2013.08.037 (2013).
880 5 Lambert, S. A. *et al.* The Human Transcription Factors. *Cell* **172**, 650-665,
881 doi:10.1016/j.cell.2018.01.029 (2018).
882 6 Vaquerizas, J. M., Kummerfeld, S. K., Teichmann, S. A. & Luscombe, N. M. A census of
883 human transcription factors: function, expression and evolution. *Nature reviews. Genetics*
884 **10**, 252-263, doi:10.1038/nrg2538 (2009).
885 7 Pierson, E. *et al.* Sharing and Specificity of Co-expression Networks across 35 Human
886 Tissues. *PLoS Comput Biol* **11**, e1004220, doi:10.1371/journal.pcbi.1004220 (2015).

887 8 Sonawane, A. R. *et al.* Understanding Tissue-Specific Gene Regulation. *Cell Rep* **21**,
888 1077-1088, doi:10.1016/j.celrep.2017.10.001 (2017).
889 9 Saha, A. *et al.* Co-expression networks reveal the tissue-specific regulation of transcription
890 and splicing. *Genome research* **27**, 1843-1858, doi:10.1101/gr.216721.116 (2017).
891 10 Boyle, A. P. *et al.* Comparative analysis of regulatory information and circuits across
892 distant species. *Nature* **512**, 453-456, doi:10.1038/nature13668 (2014).
893 11 Ray, D. *et al.* RNA-binding proteins that lack canonical RNA-binding domains are rarely
894 sequence-specific. *Sci Rep* **13**, 5238, doi:10.1038/s41598-023-32245-9 (2023).
895 12 Zeke, A. *et al.* Deep structural insights into RNA-binding disordered protein regions.
896 *Wiley Interdiscip Rev RNA* **13**, e1714, doi:10.1002/wrna.1714 (2022).
897 13 Zaharias, S. *et al.* Intrinsically disordered electronegative clusters improve stability and
898 binding specificity of RNA-binding proteins. *J Biol Chem* **297**, 100945,
899 doi:10.1016/j.jbc.2021.100945 (2021).
900 14 Kribelbauer, J. F., Rastogi, C., Bussemaker, H. J. & Mann, R. S. Low-Affinity Binding Sites
901 and the Transcription Factor Specificity Paradox in Eukaryotes. *Annu Rev Cell Dev Biol*
902 **35**, 357-379, doi:10.1146/annurev-cellbio-100617-062719 (2019).
903 15 Neph, S. *et al.* Circuitry and dynamics of human transcription factor regulatory networks.
904 *Cell* **150**, 1274-1286, doi:10.1016/j.cell.2012.04.040 (2012).
905 16 Marbach, D. *et al.* Tissue-specific regulatory circuits reveal variable modular
906 perturbations across complex diseases. *Nature methods* **13**, 366-370,
907 doi:10.1038/nmeth.3799 (2016).
908 17 Fagny, M. *et al.* Exploring regulation in tissues with eQTL networks. *Proc Natl Acad Sci*
909 *U S A* **114**, E7841-E7850, doi:10.1073/pnas.1707375114 (2017).
910 18 Agarwal, V. *et al.* Massively parallel characterization of transcriptional regulatory elements.
911 *Nature*, doi:10.1038/s41586-024-08430-9 (2025).
912 19 Avsec, Z. *et al.* Effective gene expression prediction from sequence by integrating long-
913 range interactions. *Nature methods* **18**, 1196-1203, doi:10.1038/s41592-021-01252-x
914 (2021).
915 20 Tasaki, S., Gaiteri, C., Mostafavi, S. & Wang, Y. Deep learning decodes the principles of
916 differential gene expression. *Nat Mach Intell* **2**, 376-386, doi:10.1038/s42256-020-0201-
917 6 (2020).
918 21 Osato, N. & Hamada, M. Systematic discovery of directional regulatory motifs associated
919 with human insulator sites. *bioRxiv*, doi:https://doi.org/10.1101/2024.01.20.573595
920 (2025).
921 22 Obayashi, T., Kodate, S., Hibara, H., Kagaya, Y. & Kinoshita, K. COXPRESdb v8: an
922 animal gene coexpression database navigating from a global view to detailed investigations.

Nucleic acids research **51**, D80-D87, doi:10.1093/nar/gkac983 (2023).

23 Yang, S. *et al.* COEXPEDIA: exploring biomedical hypotheses via co-expressions associated with medical subject headings (MeSH). *Nucleic acids research* **45**, D389-D396, doi:10.1093/nar/gkw868 (2017).

24 Zhu, Q. *et al.* Targeted exploration and analysis of large cross-platform human transcriptomic compendia. *Nature methods* **12**, 211-214, 213 p following 214, doi:10.1038/nmeth.3249 (2015).

25 Miller, H. E. & Bishop, A. J. R. Correlation AnalyzeR: functional predictions from gene co-expression correlations. *BMC Bioinformatics* **22**, 206, doi:10.1186/s12859-021-04130-7 (2021).

26 Raina, P. *et al.* GeneFriends: gene co-expression databases and tools for humans and model organisms. *Nucleic acids research* **51**, D145-D158, doi:10.1093/nar/gkac1031 (2023).

27 Stuart, J. M., Segal, E., Koller, D. & Kim, S. K. A gene-coexpression network for global discovery of conserved genetic modules. *Science (New York, N.Y.)* **302**, 249-255, doi:10.1126/science.1087447 (2003).

28 Lemoine, G. G., Scott-Boyer, M. P., Ambroise, B., Perin, O. & Droit, A. GWENA: gene co-expression networks analysis and extended modules characterization in a single Bioconductor package. *BMC Bioinformatics* **22**, 267, doi:10.1186/s12859-021-04179-4 (2021).

29 Warde-Farley, D. *et al.* The GeneMANIA prediction server: biological network integration for gene prioritization and predicting gene function. *Nucleic acids research* **38**, W214-220, doi:10.1093/nar/gkq537 (2010).

30 Wong, A. K., Krishnan, A. & Troyanskaya, O. G. GIANT 2.0: genome-scale integrated analysis of gene networks in tissues. *Nucleic acids research* **46**, W65-W70, doi:10.1093/nar/gky408 (2018).

31 UniProt, C. UniProt: the Universal Protein Knowledgebase in 2025. *Nucleic acids research* **53**, D609-D617, doi:10.1093/nar/gkae1010 (2025).

32 Tak Leung, R. W., Jiang, X., Chu, K. H. & Qin, J. ENPD - A Database of Eukaryotic Nucleic Acid Binding Proteins: Linking Gene Regulations to Proteins. *Nucleic acids research* **47**, D322-D329, doi:10.1093/nar/gky1112 (2019).

33 Shrikumar, A., Greenside, P. & Kundaje, A. in *Proceedings of the 34th International Conference on Machine Learning* Vol. 70 (eds Precup Doina & Teh Yee Whye) 3145--3153 (PMLR, Proceedings of Machine Learning Research, 2017).

34 Ashburner, M. *et al.* Gene ontology: tool for the unification of biology. The Gene Ontology Consortium. *Nature genetics* **25**, 25-29, doi:10.1038/75556 (2000).

35 Gene Ontology, C. *et al.* The Gene Ontology knowledgebase in 2023. *Genetics* **224**, doi:10.1093/genetics/iyad031 (2023).

36 Thomas, P. D. *et al.* PANTHER: Making genome-scale phylogenetics accessible to all. *Protein Sci* **31**, 8-22, doi:10.1002/pro.4218 (2022).

37 Hu, M. *et al.* Evaluation of large language models for discovery of gene set function. *Nature methods* **22**, 82-91, doi:10.1038/s41592-024-02525-x (2025).

38 Farshadi, E., van der Horst, G. T. J. & Chaves, I. Molecular Links between the Circadian Clock and the Cell Cycle. *J Mol Biol* **432**, 3515-3524, doi:10.1016/j.jmb.2020.04.003 (2020).

39 Snel, B., Lehmann, G., Bork, P. & Huynen, M. A. STRING: a web-server to retrieve and display the repeatedly occurring neighbourhood of a gene. *Nucleic acids research* **28**, 3442-3444, doi:10.1093/nar/28.18.3442 (2000).

40 Szklarczyk, D. *et al.* The STRING database in 2023: protein-protein association networks and functional enrichment analyses for any sequenced genome of interest. *Nucleic acids research* **51**, D638-D646, doi:10.1093/nar/gkac1000 (2023).

41 Tian, W. *et al.* Bioinformatics analysis of the role of aldolase A in tumor prognosis and immunity. *Sci Rep* **12**, 11632, doi:10.1038/s41598-022-15866-4 (2022).

42 Zhang, F. *et al.* Elevated transcriptional levels of aldolase A (ALDOA) associates with cell cycle-related genes in patients with NSCLC and several solid tumors. *BioData Min* **10**, 6, doi:10.1186/s13040-016-0122-4 (2017).

43 Zlacka, J. & Zeman, M. Glycolysis under Circadian Control. *Int J Mol Sci* **22**, doi:10.3390/ijms222413666 (2021).

44 Yang, Y., Pu, J. & Yang, Y. Glycolysis and chemoresistance in acute myeloid leukemia. *Heliyon* **10**, e35721, doi:10.1016/j.heliyon.2024.e35721 (2024).

45 Puram, R. V. *et al.* Core Circadian Clock Genes Regulate Leukemia Stem Cells in AML. *Cell* **165**, 303-316, doi:10.1016/j.cell.2016.03.015 (2016).

46 Lee, Y. Roles of circadian clocks in cancer pathogenesis and treatment. *Exp Mol Med* **53**, 1529-1538, doi:10.1038/s12276-021-00681-0 (2021).

47 Liberti, M. V. & Locasale, J. W. The Warburg Effect: How Does it Benefit Cancer Cells? *Trends Biochem Sci* **41**, 211-218, doi:10.1016/j.tibs.2015.12.001 (2016).

48 Vander Heiden, M. G., Cantley, L. C. & Thompson, C. B. Understanding the Warburg effect: the metabolic requirements of cell proliferation. *Science (New York, N.Y.)* **324**, 1029-1033, doi:10.1126/science.1160809 (2009).

49 Semenza, G. L. Hypoxia-inducible factors: mediators of cancer progression and targets for cancer therapy. *Trends Pharmacol Sci* **33**, 207-214, doi:10.1016/j.tips.2012.01.005 (2012).

50 Keith, B., Johnson, R. S. & Simon, M. C. HIF1alpha and HIF2alpha: sibling rivalry in hypoxic tumour growth and progression. *Nat Rev Cancer* **12**, 9-22, doi:10.1038/nrc3183 (2011).

51 Uhlen, M. *et al.* Proteomics. Tissue-based map of the human proteome. *Science (New York, N.Y.)* **347**, 1260419, doi:10.1126/science.1260419 (2015).

52 Israelsen, W. J. & Vander Heiden, M. G. Pyruvate kinase: Function, regulation and role in cancer. *Semin Cell Dev Biol* **43**, 43-51, doi:10.1016/j.semcdb.2015.08.004 (2015).

53 Bluemlein, K. *et al.* No evidence for a shift in pyruvate kinase PKM1 to PKM2 expression during tumorigenesis. *Oncotarget* **2**, 393-400, doi:10.18632/oncotarget.278 (2011).

54 Wang, X. & Liu, L. AKAP8 interacting with DDX5 to regulate R-loop balance involves in lung carcinoma cell growth. *bioRxiv*, doi:10.1101/2023.11.28.568985 (2024).

55 Shirai, Y., Suwa, T., Kobayashi, M., Koyasu, S. & Harada, H. DDX5 enhances HIF - 1 activity by promoting the interaction of HIF - 1α with HIF - 1β and recruiting the resulting heterodimer to its target gene loci. *Biology of the Cell* **116**, doi:10.1111/boc.202300077 (2023).

56 Leszczynska, K. B. *et al.* Hypoxia - mediated regulation of DDX5 through decreased chromatin accessibility and post - translational targeting restricts R - loop accumulation. *Molecular Oncology* **17**, 1173-1191, doi:10.1002/1878-0261.13431 (2023).

57 Farshadi, E., van der Horst, G. T. J. & Chaves, I. Molecular Links between the Circadian Clock and the Cell Cycle. *Journal of Molecular Biology* **432**, 3515-3524, doi:10.1016/j.jmb.2020.04.003 (2020).

58 Ran, J. *et al.* Hypoxia regulates glycolysis through the HIF-1α/BMAL1/ALDOC axis to reduce oxaliplatin sensitivity in colorectal cancer. *Journal of Cancer* **16**, 2503-2515, doi:10.7150/jca.108582 (2025).

59 De Vitis, C. *et al.* ALDOC- and ENO2- driven glucose metabolism sustains 3D tumor spheroids growth regardless of nutrient environmental conditions: a multi-omics analysis. *Journal of Experimental & Clinical Cancer Research* **42**, doi:10.1186/s13046-023-02641-0 (2023).

60 Minchenko, O. H., Garmash, I. A. & Minchenko, D. O. Inhibition of IRE1 modifies hypoxic regulation of G6PD, GPI, TKT, TALDO1, PGLS and RPIA genes expression in U87 glioma cells. *The Ukrainian Biochemical Journal* **89**, 38-49, doi:10.15407/ubj89.01.038 (2017).

61 Obeidat, N. *et al.* Effects of cyclic acute and chronic hypoxia on the expression levels of metabolism related genes in a pancreatic cancer cell line. *Biomedical Reports* **17**, doi:10.3892/br.2022.1564 (2022).

62 Ladomery, M. Multifunctional proteins suggest connections between transcriptional and

1031 post-transcriptional processes. *Bioessays* **19**, 903-909, doi:10.1002/bies.950191010
1032 (1997).
1033 63 Kim, S., Yu, N. K. & Kaang, B. K. CTCF as a multifunctional protein in genome regulation
1034 and gene expression. *Exp Mol Med* **47**, e166, doi:10.1038/emm.2015.33 (2015).
1035 64 Osato, N. Characteristics of functional enrichment and gene expression level of human
1036 putative transcriptional target genes. *BMC Genomics* **19**, 957, doi:10.1186/s12864-017-
1037 4339-5 (2018).
1038 65 Burley, S. K. & Kamada, K. Transcription factor complexes. *Curr Opin Struct Biol* **12**, 225-
1039 230, doi:10.1016/s0959-440x(02)00314-7 (2002).
1040 66 Goos, H. *et al.* Human transcription factor protein interaction networks. *Nat Commun* **13**,
1041 766, doi:10.1038/s41467-022-28341-5 (2022).
1042 67 Berenson, A. *et al.* Paired yeast one-hybrid assays to detect DNA-binding cooperativity
1043 and antagonism across transcription factors. *Nat Commun* **14**, 6570, doi:10.1038/s41467-
1044 023-42445-6 (2023).
1045 68 Barrett, T. *et al.* NCBI GEO: archive for functional genomics data sets--update. *Nucleic*
1046 *acids research* **41**, D991-995, doi:10.1093/nar/gks1193 (2013).
1047 69 Edgar, R., Domrachev, M. & Lash, A. E. Gene Expression Omnibus: NCBI gene
1048 expression and hybridization array data repository. *Nucleic acids research* **30**, 207-210,
1049 doi:10.1093/nar/30.1.207 (2002).
1050 70 Kolmykov, S. *et al.* GTRD: an integrated view of transcription regulation. *Nucleic acids*
1051 *research* **49**, D104-D111, doi:10.1093/nar/gkaa1057 (2021).
1052 71 Hinrichs, A. S. *et al.* The UCSC Genome Browser Database: update 2006. *Nucleic acids*
1053 *research* **34**, D590-598, doi:10.1093/nar/gkj144 (2006).
1054 72 Mudge, J. M. *et al.* GENCODE 2025: reference gene annotation for human and mouse.
1055 *Nucleic acids research* **53**, D966-D975, doi:10.1093/nar/gkae1078 (2025).
1056 73 Van Nostrand, E. L. *et al.* A large-scale binding and functional map of human RNA-
1057 binding proteins. *Nature* **583**, 711-719, doi:10.1038/s41586-020-2077-3 (2020).
1058 74 Young Cheon, N., Kim, S. & Yil Lee, J. in *Gene Expression* Ch. Chapter 3,
1059 (IntechOpen, 2022).
1060 75 Gasperini, M. *et al.* A Genome-wide Framework for Mapping Gene Regulation via
1061 Cellular Genetic Screens. *Cell* **176**, 1516, doi:10.1016/j.cell.2019.02.027 (2019).
1062 76 Tan, X. *et al.* Novel Insights into the Circadian Rhythms Based on Long Noncoding and
1063 Circular RNA Profiling. *Int J Mol Sci* **25**, doi:10.3390/ijms25021161 (2024).
1064 77 Poelmans, G., Franke, B., Pauls, D. L., Glennon, J. C. & Buitelaar, J. K. AKAPs integrate
1065 genetic findings for autism spectrum disorders. *Transl Psychiatry* **3**, e270,
1066 doi:10.1038/tp.2013.48 (2013).

1067